Experimental Thermal and Fluid Science 54 (2014) 304–312

Contents lists available at ScienceDirect

Experimental Thermal and Fluid Science

journal homepage: www.elsevier.com/locate/etfs

Performance evaluation of a tube-in-tube CO_2 gas cooler used in a heat pump water heater

Pei-Yu Yu [a,b], Wei-Keng Lin [b], Chi-Chuan Wang [c,*]

[a] Green Energy and Environment Research Laboratories, Industrial Technology Research Institute, Taiwan
[b] Department of Engineering and System Science, National Tsing Hua University, Taiwan
[c] Department of Mechanical Engineering, National Chiao Tung University, Taiwan

ARTICLE INFO

Article history:
Received 13 November 2013
Received in revised form 9 January 2014
Accepted 13 January 2014
Available online 24 January 2014

Keywords:
Carbon dioxide
Supercritical
Gas cooler
Tube-in-tube heat exchanger

ABSTRACT

In this study, investigation of the performance of a tube-in-tube counter-flow water-cooled CO_2 gas cooler operating above and near critical pressure is presented using a heat pump water heater with CO_2 flowing in the annulus side. A tube-in-tube heat exchanger model applicable for supercritical fluid CO_2 and water was also developed and validated. The measured total heat transfer capacity ranged from 1.31 to 4.06 kW at various test conditions. The calculations show good agreement with the experimental results. The results demonstrate that the variation of CO_2 temperature tends to show very slow decreasing near the pseudo-critical region when compared to the inlet region. Yet this phenomenon becomes more pronounced as the inlet pressure is close to the critical pressure (73.8 bar). The calculation also reveals a peculiar phenomenon that the local heat transfer rate of the heat exchanger peaks within the heat exchanger near the pseudo critical region due to the drastic rise of specific heat (C_P value).

1. Introduction

For the past several decades, revisit of refrigerant CO_2 was strongly taken into consideration as a candidate for replacing the synthetic refrigerants like HFCs. CO_2 features advantages such as ecology benign, safety and inexpensive cost [1,2]. However, with its relatively low critical temperature (31.1 °C), CO_2 is often operated as a supercritical fluid for a typical vapor compression cycle under normal operating conditions, thereby leading to a so-called transcritical cycle [3–5]. Mobile air conditioning, residential AC/heat pump systems and military environmental control units (ECUs) are typical examples exploiting CO_2 transcritical cycle applications. Moreover, it was found that CO_2 water heat pump could outperform conventional refrigerants in terms of system COP [6]. The continuous and large temperature glide for CO_2 in a transcritical process can contribute to improve the performance of heating tape water.

Gas cooler, in which CO_2 is cooled with persistent temperature drop, is different from those constant temperature condensation processes, and it is one of most important device in CO_2 transcritical cycle since its flow arrangements and behaviors can greatly affect the optimal operating pressure and system efficiency. Many literature had been presented on various gas cooler models for space heating, cooling and water heating [3,7–10]. Most of studies used the gas cooler model to enhance the system performance of a refrigeration plant or heat pump [11–14]; however, only a few of researches devoted component-level behavior of gas coolers particularly for water heating applications. Sanchez et al. [15] presented a water–CO_2 coaxial heat exchanger model with refrigerant flowing through internal tube bundle using finite volume technique and CO_2 convective coefficient correlations. Their results revealed that thermal effectiveness increases with the rise of refrigerant pressure and water mass flow rate, and decreases with the increase of evaporating pressure and water inlet temperature. Fronk and Garimella [4,5] carried out an analysis of a water-coupled gas cooler with a compact, multi-pass cross-counter flow of aluminum brazed plate, microchannel CO_2 gas cooler, and the model was validated with experimental data. REFPROP [16] presented an analysis for a concentric counter-flow heat exchanger by solving a set of complicated partial differential equations, including conservation of mass, momentum and energy amid CO_2 and water and considering the wall conduction in both radial and axial direction. They found that the variation of the local heat flux revealed a local maximum within the heat exchanger due to the tremendous change of specific heat of CO_2.

In a liquid-cooled gas cooler, the contribution of CO_2 thermophysical changes is more important than that in an air-cooled one due to air-side thermal resistance is dominant in the air-cooled heat exchangers. But, investigations concerning the water-cooled gas cooler are comparatively fewer. Therefore, the objective

* Corresponding author. Address: Department of Mechanical Engineering, National Chiao Tung University, EE474, 1001 University Road, Hsinchu 300, Taiwan. Tel.: +886 3 5712121x55105.
E-mail address: ccwang@mail.nctu.edu.tw (C.-C. Wang).

0894-1777/$ - see front matter © 2014 Elsevier Inc. All rights reserved.
http://dx.doi.org/10.1016/j.expthermflusci.2014.01.007

Nomenclature

A	surface area (m^2)
C	heat capacity flow rate ($W K^{-1}$)
$\bar{C}$	average heat capacity flow rate ($W K^{-1}$)
Cp	specific heat ($J kg^{-1} K^{-1}$)
d	diameter (m)
f	friction factor
h	heat transfer coefficient ($W m^{-2} K^{-1}$)
i	specific enthalpy ($kJ kg^{-1}$)
ID	inner diameter (m)
k	conductivity ($W m^{-1} K^{-1}$)
L	tube length (m)
$LMTD$	log mean temperature difference (K)
$\dot{m}$	mass flow rate ($kg s^{-1}$)
Nu	Nusselt number (hd/k)
OD	outer diameter (m)
P	pressure (MPa)
Pr	Prandtl number
Q	heat transfer rate (kW)
R	thermal resistance ($°C W^{-1}$)
Re	Reynolds number ($\rho ud/\mu$)
T	temperature (°C)
u	velocity ($m s^{-1}$)
U	overall heat transfer coefficient ($W m^{-2} K^{-1}$)

Greek letters

ΔT	temperature difference (K)
Δ	maximum temperature difference of gas cooler, $=T_{c,i}-T_{w,i}$
μ	viscosity ($kg m^{-1} s^{-1}$)
ρ	density ($kg m^{-3}$)

Subscripts

b	bulk
c	carbon dioxide
c, i	ith segment of carbon dioxide
f	film
H	hydraulic diameter
i	inner
i	ith segment of heat exchanger
max	larger one
min	smaller one
o	outer
w	water
$wall$	wall
w, i	ith segment of water side

of this study is to develop a simple counter-flow heat exchanger model capable to analyze the heat transfer behavior of CO_2 tube-in-tube water-cooled gas cooler subject to refrigerant flowing in annulus side both numerically and experimentally.

2. Numerical method

The model heat exchanger is a double-pipe heat exchanger with CO_2 flowing through the annulus whereas the water is flowing counter-currently in the tube side. Fig. 1 is a schematic of the heat exchanger. Since considerable change of physical properties of CO_2 may occur especially nearby pseudo-critical temperatures, the heat exchanger must be subdivided into many small segments. A prior sensitive analysis of the influence of segments was performed, and a total of 26 segments were used in this simulation. Higher number of control volumes produces smaller errors but increases the calculation time. A number of finite volumes between 20 and 30 optimize the calculation time and the error [15]. A schematic diagram showing the variation of temperature for CO_2 and water is shown in Fig. 1(b) where the subscript c denotes CO_2 and w represents water. In this regard, the heat balance amid water and coolant in each segment i can be written in the following equations:

$$Q_i = m_c Cp_{c,i}(T_{c,i} - T_{c,i+1}) = m_w Cp_{w,i}(T_{w,i} - T_{w,i+1}). \quad (1)$$

$$Q_i = (UA)_i \times (LMTD)_i. \quad (2)$$

The overall heat transfer coefficient is obtained from

$$\frac{1}{UA} = \frac{1}{h_c A_{o,i}} + \frac{\ln \frac{d_o}{d_i}}{2\pi k_{wall} L} + \frac{1}{h_w A_{i,i}}. \quad (3)$$

The physical properties for CO_2 are a function of local pressure and temperature and the properties of water are related to local temperature. The relevant properties are obtained from REFPROP 8.0 (2007) [16]. The heat transfer coefficient of CO_2 is based on the Dang and Hihara correlation (2004) [7], i.e.

$$h_c = Nu_c k_c / d_H, \quad (4)$$

$$Nu_c = \frac{\left(\frac{f_c}{8}\right)(\mathrm{Re}_b - 1000)\mathrm{Pr}}{1.07 + 12.7\sqrt{\frac{f_c}{8}}\left(\mathrm{Pr}^{2/3} - 1\right)}, \quad (5)$$

where

$$\mathrm{Pr} = \begin{cases} Cp_b\mu_b/\lambda_b, & \text{for } Cp_b \geq \overline{Cp}, \\ \overline{Cp}_b\mu_b/\lambda_f, & \text{for } Cp_b < \overline{Cp} \text{ and } \mu_b/\lambda_b \geq \mu_f/\lambda_f, \\ \overline{Cp}_b\mu_f/\lambda_f, & \text{for } Cp_b < \overline{Cp} \text{ and } \mu_b/\lambda_b < \mu_f/\lambda_f, \end{cases} \quad (6)$$

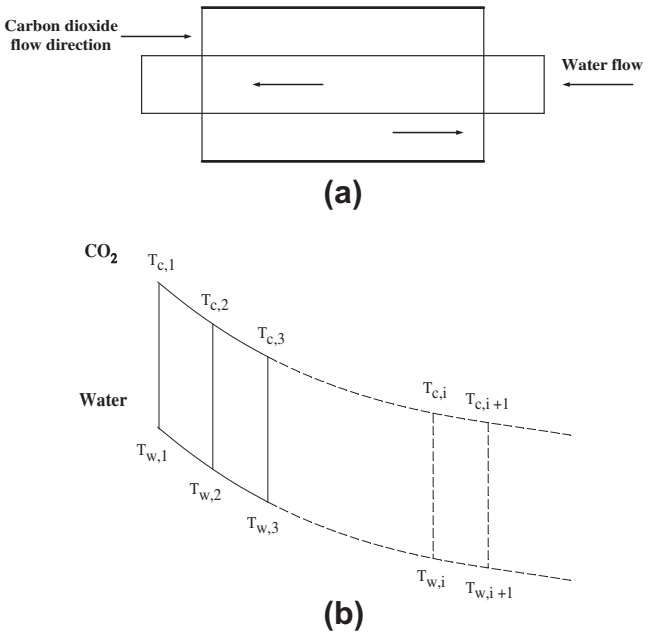

Fig. 1. (a) Schematic of the tube-in-tube heat exchanger and (b) definition of the temperature variation for CO_2 and water alongside the length of the tube-in-tube heat exchanger.

$$\overline{Cp} = \frac{h_b - h_{wall}}{T_b - T_{wall}}, \tag{7}$$

$$\mathrm{Re}_b = \frac{Gd_H}{\mu_b}, \tag{8}$$

$$f_c = [1.82\log(\mathrm{Re}_b) - 1.64]^{-2}, \tag{9}$$

where the subscript b represents the bulk temperature, and *wall* is evaluated at the wall temperature and f denotes calculation at the film temperature. The film temperature, T_f, is defined as $T_f = (T_b + T_{wall})/2$. On the other hand, the heat transfer coefficient for the water side, h_w, is via Gnielinski (1976) correlation [17]:

$$h_w = Nu_w k_w/d, \tag{10}$$

$$Nu_w = \frac{\left(\frac{f_w}{8}\right)(\mathrm{Re} - 1000)\mathrm{Pr}}{1.07 + 12.7\sqrt{\frac{f_w}{8}}\left(\mathrm{Pr}^{2/3} - 1\right)}, \tag{11}$$

where

$$f_w = [1.82\log(\mathrm{Re}_w) - 1.64]^{-2}. \tag{12}$$

In this study, CO_2 is as a supercritical working fluid which distinguishing feature is dramatically rapid variations of its physical properties as the temperature is closed to the pseudocritical point. The definition of pseudocritical temperature T_{pc} is the temperature at which the specific heat reaches a peak for a given pressure. The pseudocritical temperature T_{pc} of CO_2 is a function of pressure and can be best fitted by the following algebraic equation based on the data from NIST Refrigerants Database REFPROP [18].

$$T_{pc} = -122.6 + 6.124P - 0.1657P^2 + 0.01773P^{2.5} - 0.0005608P^3, \tag{13}$$

where the pseudocritical temperature T_{pc} is in °C and the pressure p is in bar.

3. Experimental setup

3.1. Experimental apparatus and procedures

Fig. 2 shows a schematic diagram of the closed test loop which is modified with a water-to-water type of heat pump water heater. A variable speed compressor was used to circulate CO_2 refrigerant and maintain the inlet pressure of the test section (gascooler) at assigned high pressures. Water enters the gascooler to cool down CO_2 with the counter-flow arrangement and it was controlled at selected flow rate by a pump and regulated valves. After passing through a Coriolis-type mass flow meter, CO_2 was cooled in the internal heat exchanger and the superheat of CO_2 in the suction side is increased before returning to the compressor. The electronic

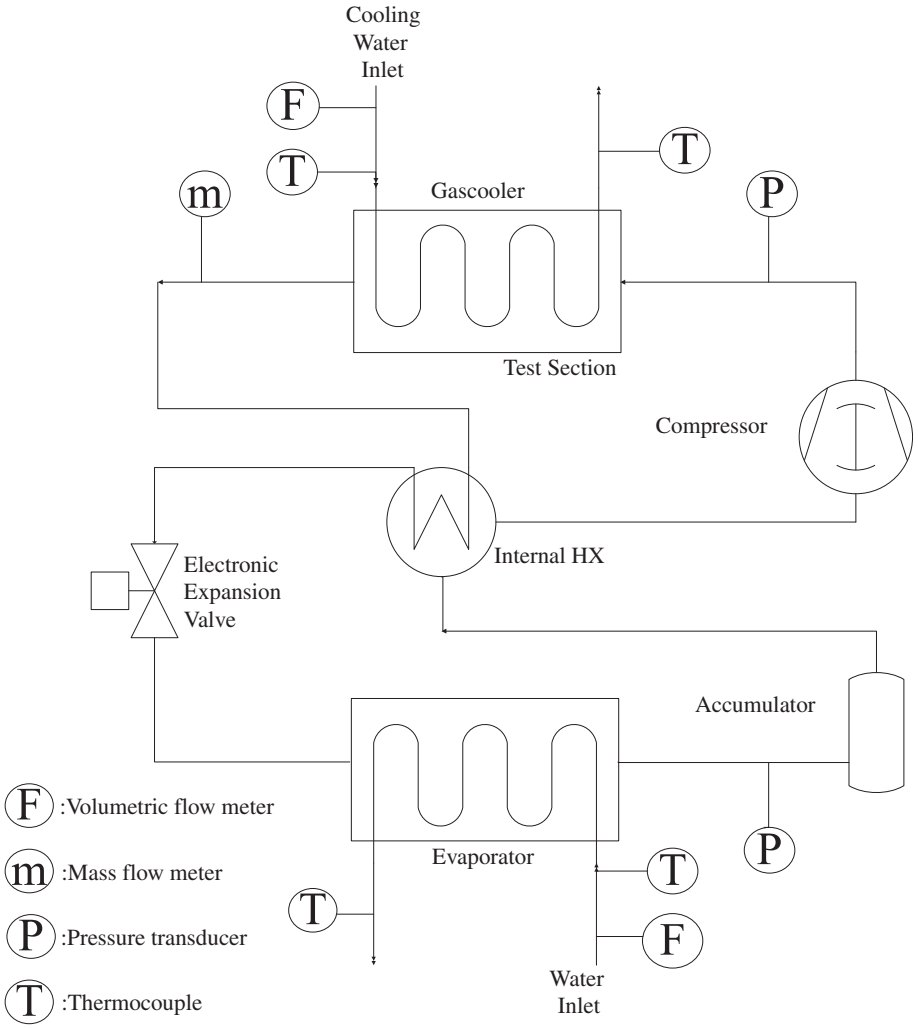

Fig. 2. Schematic diagram of the closed test loop.

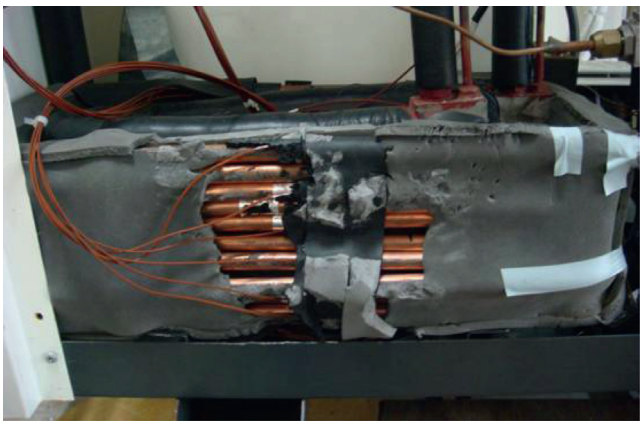

Fig. 3. Photograph and schematic of the gas cooler.

expansion valve was driven by a stepping motor and the stainless steel valve body sustained a maximum working pressure of 150 bar. The opening of the valve ranged is controlled by pulse signal with 480 pulses representing fully opened. Like the gascooler, a double tube type water-coupled heat exchanger served as the evaporator. CO_2 is then evaporated to complete the full refrigeration cycle. Chilled water flowing through the evaporator is used as the heat source to absorb heat from CO_2. To prevent liquid refrigerant from entering the compressor, an accumulator having U-shape type was installed between the evaporator and the internal heat exchanger.

Fig. 3 depicts the configuration of the test section (gascooler) which is consisted of a 13 m-long spiral tube-in-tube counter-flow heat exchanger. The CO_2 flows through the outer annular passage from the top while cooling water flows inside the inner tube. The gascooler was made of smooth copper with inner diameter of 6.34 mm and a thickness of 0.8 mm in the inner tube. The inside diameter of the outer tube is 10 mm and thickness is 1.0 mm with a subsequent annular gap of 1.03 mm between inner tube and outer tube. The test section was covered with a 12.7 mm thick rubber insulation to minimize heat dissipation into the ambient environment. The wall temperature of the outer tube was measured at 13 locations is equally distributed along the gascooler with using T-type thermocouples taped on the outside wall. The inlet and outlet temperatures of the cooling water were gauged with Pt 100 sensors to determine the total heat transfer capacity in the test section.

Table 2
Test conditions of the gas cooler (CO_2 side).

Parameter	Value
Inlet pressure of CO_2 (bar)	96, 86, 76
Inlet temperature of water (°C)	15, 20, 25, 30
Volumetric flow rate of water (L min^{-1})	1.0, 1.5, 2.0

3.2. Uncertainty analysis

The uncertainty in this study is determined with ISO/IEC Guide to the expression of uncertainty in measurement [19]. An example of uncertainty analysis also was demonstrated to determine the uncertainty in an experimental statistics [20].

According to the definition of ISO GUM,

$$Y = y \pm U, \tag{14}$$

$$U = k \cdot u_c(y), \tag{15}$$

where Y: measurand; y: estimate of measurand; U: expanded uncertainty; $u_c(y)$: combined standard uncertainty;

$$u_c^2(y) = \sum_{i=1}^{n} \left[\frac{\partial f}{\partial x_i}\right]^2 u^2(x_i), \tag{16}$$

where $u_c(y)$ is combined standard uncertainty, $u(x_i)$ is standard uncertainty and x_i are the error sources which affect the estimation of measurand y, as shown below:

$$y = f(x_i). \tag{17}$$

Table 1 is a list of the combined standard uncertainties in this study and instrumentation calibration is the important sources of uncertainty for each parameter of measurement. A coverage factor of 2 multiplied by the values in the Table 2 gives a 95% confidence level that the actual uncertainty is less than or equal to the stated uncertainty [20].

3.3. Test conditions

Table 2 shows the test conditions in the present work and all experiment was executed in an ISO 17025 certified laboratory. Experiments were conducted for three different inlet pressures of carbon dioxide from 76 to 96 bar by tuning a variable speed compressor and the opening of an electrical expansion valve. The inlet temperatures of water were adjusted from 15° to 30° centigrade. The water volumetric flow rates were controlled from 1.0 to

Table 1
Summary of the combined standard uncertainties for the measured parameters.

Parameter	Major source of uncertainty	Magnitude of uncertainty
Measuring instrumentation		
1. Water volume flow rate	Instrumentation calibration	±1% (Yokogawa AXF)
2. CO_2 mass flow rate	Instrumentation calibration	±0.35% (Micro Motion)
3. CO_2 temperature	Instrumentation calibration	±1 °C (T-type thermocouple)
4. Water temperature	Instrumentation calibration	±0.1 °C (Pt100 RTD)
5. CO_2 absolute pressure	Instrumentation calibration	±0.3% (Yokogawa PT)

Table 3
Measured data of the 36 test conditions.

Water inlet condition (Q)	$T_{c,in}$ (°C)	$P_{c,in}$ (bar)	$T_{w,in}$ (°C)	$\dot{m}_c$ (kg s^{-1})	$\dot{m}_w$ (kg s^{-1})	Calculated (Q) (Watt)	Measured Q (Watt)	Deviation (%)
P = 96 bar								
15 °C/1.0LPM	91.8	95.9	15.0	0.0135	0.0172	1985.97	2164	−8.23
15 °C/1.5LPM	83.3	95.9	15.0	0.0137	0.0249	3109.01	2988	4.07
15 °C/2.0LPM	79.9	96.5	14.9	0.0136	0.0332	3468.41	3662	−5.29
20 °C/1.0LPM	92.9	96.2	20.0	0.0135	0.0166	2078.07	1867	11.29
20 °C/1.5LPM	86.9	96.0	20.1	0.0134	0.0245	2644.67	2539	4.16
20 °C/2.0LPM	82.4	96.3	20.1	0.0134	0.0332	2978.29	3112	−4.28
25 °C/1.0LPM	94.5	96.4	25.0	0.0136	0.0163	1826.53	1556	17.39
25 °C/1.5LPM	91.9	96.1	25.1	0.0130	0.0247	1978.07	2021	−2.13
25 °C/2.0LPM	85.3	96.3	25.0	0.0132	0.0334	2436.62	2380	2.37
30 °C/1.0LPM	92.1	96.0	29.9	0.0139	0.0157	1448.03	1312	10.35
30 °C/1.5LPM	92.1	96.1	30.0	0.0130	0.0246	1284.48	1583	−18.85
30 °C/2.0LPM	89.0	96.2	30.0	0.0128	0.0337	1381.36	1671	−17.31
P = 86 bar								
15 °C/1.0LPM	78.1	86.3	15.0	0.0146	0.0160	3204.83	2895	10.69
15 °C/1.5LPM	76.3	85.9	14.9	0.0138	0.0243	3698.58	3620	2.17
15 °C/2.0LPM	72.9	86.3	15.0	0.0138	0.0345	3635.75	3811	−4.60
20 °C/1.0LPM	76.0	85.9	20.0	0.0146	0.0181	3332.00	2790	19.43
20 °C/1.5LPM	79.0	86.3	20.0	0.0134	0.0261	3463.57	3391	2.13
20 °C/2.0LPM	74.9	86.0	20.1	0.0136	0.0350	3448.66	3620	−4.74
25 °C/1.0LPM	77.9	85.9	25.0	0.0149	0.0158	2716.02	2233	21.65
25 °C/1.5LPM	76.4	85.9	25.0	0.0143	0.0245	3161.21	2887	9.51
25 °C/2.0LPM	78.9	85.9	25.1	0.0131	0.0334	3211.73	3291	−2.40
30 °C/1.0LPM	76.2	86.0	30.0	0.0149	0.0173	2446.94	2010	21.73
30 °C/1.5LPM	76.0	86.4	30.0	0.0145	0.0252	2690.47	2482	8.40
30 °C/2.0LPM	75.1	85.8	30.1	0.0142	0.0336	2948.85	2795	5.52
P = 76 bar								
15 °C/1.0LPM	59.3	76.1	15.1	0.0132	0.0157	3787.11	3560	6.38
15 °C/1.5LPM	58.6	75.8	15.1	0.0129	0.0251	3734.60	3907	−4.40
15 °C/2.0LPM	65.4	76.0	15.1	0.0130	0.0340	3628.80	4056	−10.54
20 °C/1.0LPM	60.2	75.9	20.0	0.0131	0.0159	3503.54	3252	7.75
20 °C/1.5LPM	59.6	76.1	20.1	0.0129	0.0255	3547.41	3733	−4.96
20 °C/2.0LPM	60.3	76.4	20.0	0.0125	0.0345	3445.20	3870	−10.99
25 °C/1.0LPM	60.9	75.9	24.9	0.0130	0.0157	3190.78	2934	8.74
25 °C/1.5LPM	60.7	76.1	25.0	0.0130	0.0249	3352.63	3454	−2.93
25 °C/2.0LPM	59.0	76.1	25.0	0.0129	0.0344	3287.14	3655	−10.07
30 °C/1.0LPM	61.2	75.9	30.0	0.0129	0.0171	2867.34	2553	12.32
30 °C/1.5LPM	60.6	76.2	30.1	0.0129	0.0266	3174.02	3185	−0.36
30 °C/2.0LPM	59.2	75.7	30.0	0.0128	0.0348	3075.26	3380	−9.02

2.0 L min^{-1} by a pump and regulated valves. A total of 36 experimental test conditions were carried out to investigate the performance of this gas cooler.

4. Results and discussion

The prediction of the total heat transfer capacity of the gas cooler is compared with the experimental data first. Note that the detailed experimental conditions are tabulated in Table 3. The measured results of the total heat transfer capacity ranged from 1.31 to 4.06 kW subject to various inlet pressures and water flowrate. The simulation is conducted with the same inlet conditions for CO_2 and water, and the corresponding comparison of heating capacity is depicted in Fig. 4. Deviation between the calculation and the measured data ranged from −18.85% to 21.73% over the range of refrigerant and water inlet conditions, with the highest relative deviation occurring at the lowest water flow rate and highest water inlet temperature whose details can be seen in Table 3. As shown in Fig. 4, approximate 94% of the 36 data points were predicted within the ±20% accuracy limits, indicating that the mathematical model predicts the total heat transfer capacity reasonably well. Furthermore, the difference between calculations and measurement becomes profound as the total heat transfer capacity is larger than 2.3 kW.

The total heating capacity vs. various cooling water inlet conditions at various CO_2 inlet pressures are shown in Fig. 5. The corresponding inlet pressures are 76, 86, and 96 bar respectively. The measured total heating capacity ranged from 1.31 to 4.06 kW depending on the test conditions. As seen in Fig. 5, the total heating loads are increased when the cooling water flowrate is increased or when the water inlet temperature is reduced. However, the increasing trend subject to water coolant flowrate is not the same pertaining to the rise of water flow rate. Note that the

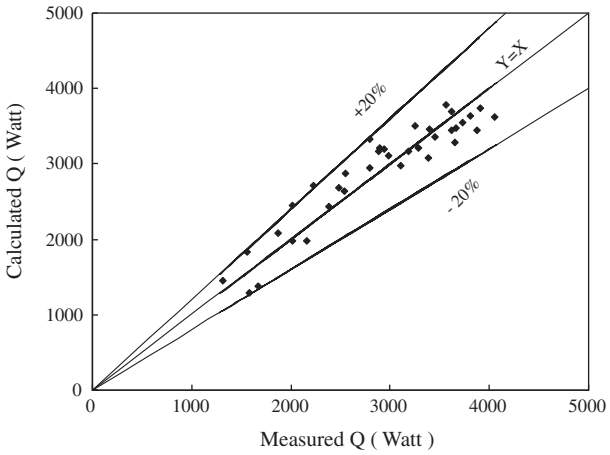

Fig. 4. Comparison of measured heating capacity against calculation.

mass flowrate of CO_2 stays roughly the same in all cases. In Fig. 5(a) where the CO_2 pressure is maintained at 76 bar, it can be found that for a lower water inlet temperature of 15 °C the heating capacity rises steadily against the water flowrate. On the other hand, only marginal rise of heating capacity vs. water flowrate is seen when the water temperature is increased to 30 °C. The heating capacity is associated with effective overall heat transfer coefficient U and the mean temperature difference between CO_2 and water. Initially, the thermal resistance in the water side is about 40–60% larger than that of CO_2 side. Therefore, normally one can expect that an increase of the water flowrate gives rise to an effective drop of total thermal resistance, and accordingly a steady rise of heating capacity. This is actually the case for a lower water inlet temperature of 15 °C. However, it appears that the rise of heating capacity subject to water flowrate is only marginal for a higher inlet water temperature of 30 °C despite the overall heat transfer coefficient still shows a noticeable rise with the water flowrate. The major explanation of this phenomenon can be made clear from Table 3 where an appreciable drop of effective temperature difference between CO_2 and water is encountered when the water inlet temperature is raised to 30 °C. It is found that the effective temperature difference is reduced by approximately 40% when the water inlet temperature is raised to 30 °C. Moreover, the maximum heat transfer rate Q_{max}, represents the maximum heat transfer rate for an infinite large heat exchanger and is given as $Q = \bar{C}_{min}\Delta$ ($\bar{C}_{min}$ represents the average capacity flowrate ($= \dot{m}\bar{C}_p$) which can be either in CO_2 side or water side depending on the corresponding effective $\bar{C}_{min}$ value and $\Delta = T_{c,in} - T_{w,in}$). Normally, $\bar{C}_{min}$ is at the CO_2 side. With the enormous change of C_p of CO_2 alsonside the heat exchanger, $\bar{C}_p$ must be integrated for the whole flow path. An estimation of Q_{max} for the inlet water temperature of 15 °C and 30 °C yields 4.2 and 1.9 kW respectively. The results suggest that the effective temperature difference plays an imperative role on the heating capacity subject to water inlet flowrate rate and temperature and the corresponding heating capacity is also limited by the Q_{max}.

Analogous trend for the heating capacity vs. water flowrate is also encountered when the inlet pressure of CO_2 is raised to 86 and 96 bar as shown in Fig. 5(b) and (c). Note that both the present calculation and Wang and Hihara [21] all indicated that the overall heat transfer coefficient decreases monotonically with the increase of CO_2 pressure [21]. The decline of overall heat transfer coefficient is mainly associated with sharp decline with thermal conductivity and heat capacity at the pseudo-critical region which results in an appreciable drop of heat transfer coefficient of CO_2. However, from Table 3, one can see an effective increase in CO_2 inlet temperature when the inlet pressure is increased, thereby the considerable rise of mean temperature difference amid water and CO_2 compensates the slight decrease in UA value, and accordingly a slight rise of effective heating capacity emerges.

The temperature distribution of CO_2 and water along the flow path at three different CO_2 inlet pressure under 2 L min^{-1} water flowrate and 15 °C water inlet temperature are shown as Fig. 6. The temperature of the CO_2 drop continuously alongside the CO_2 path, yet the temperature may pass through the pseudo-critical temperature for a given pressure and it reaches a lower temperature that is close to the water inlet temperature. This is the so-called transcritical operation. A close examination of the temperature variation of CO_2 indicates that the temperature variation of CO_2 near the pseudo-critical region is contradictory to those at the entrance region where the CO_2 temperature shows a continuous decline. In fact, the temperature drop becomes much less than that in the entrance region. This phenomenon becomes even more pronounced as the inlet pressure is decreased toward the critical point (73.8 bar). The extraordinary phenomenon is associated with the sharp change of C_P value in the neighborhood of pseudo-critical

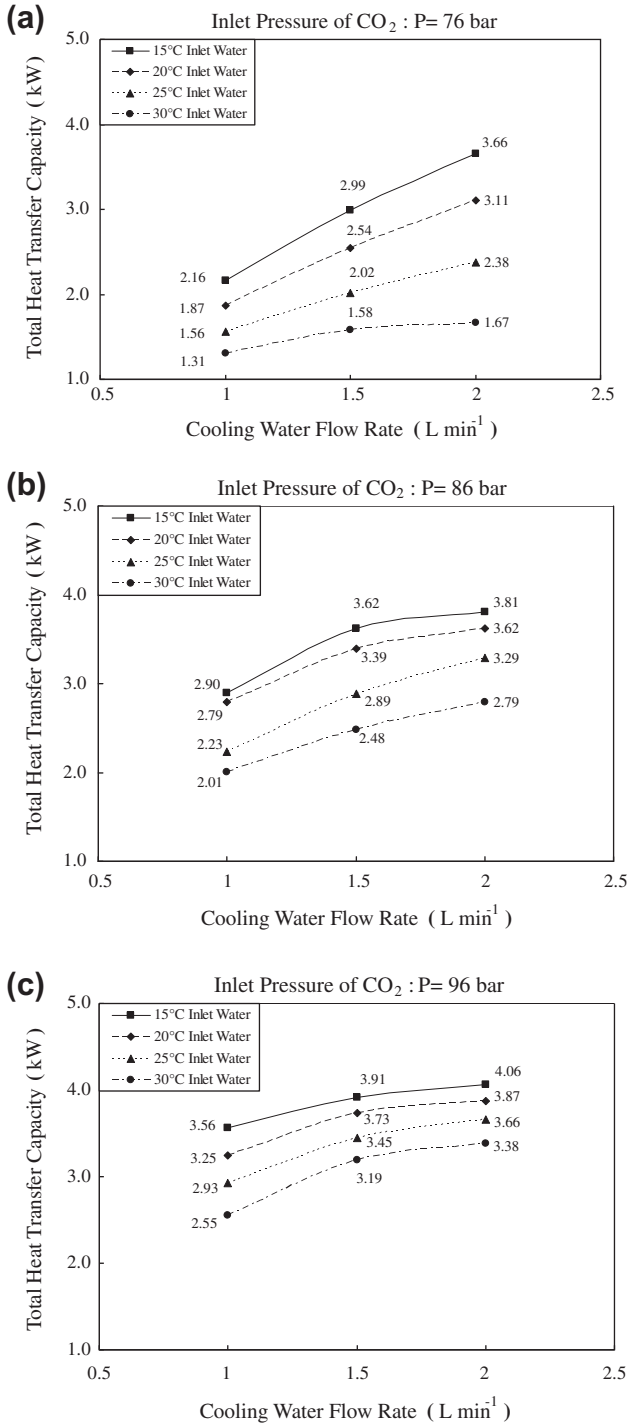

Fig. 5. Measured total heat transfer capacity vs. cooling water inlet conditions for three different CO_2 inlet pressure. (a) P = 76 bar; (b) P = 86 bar and (c) P = 96 bar.

temperature as shown Fig. 7(a). In fact, it is evitable that the high temperature CO_2 must pass through the pseudo-critical temperature during a trans-critical process. In other words, the heat capacity flow rate (C) of the CO_2 reveals a considerable rise due to a tremendous rise of C_P value around the pseudo-critical temperature. From a simple energy balance formula, $Q = C_c\Delta T$, it is not surprised that the variation of CO_2 temperature tends to be small adjacent to the pseudo-critical region when compared to that at the inlet region. The phenomenon had been theoretically calculated by Yu et al. [22], yet it is validated from the present

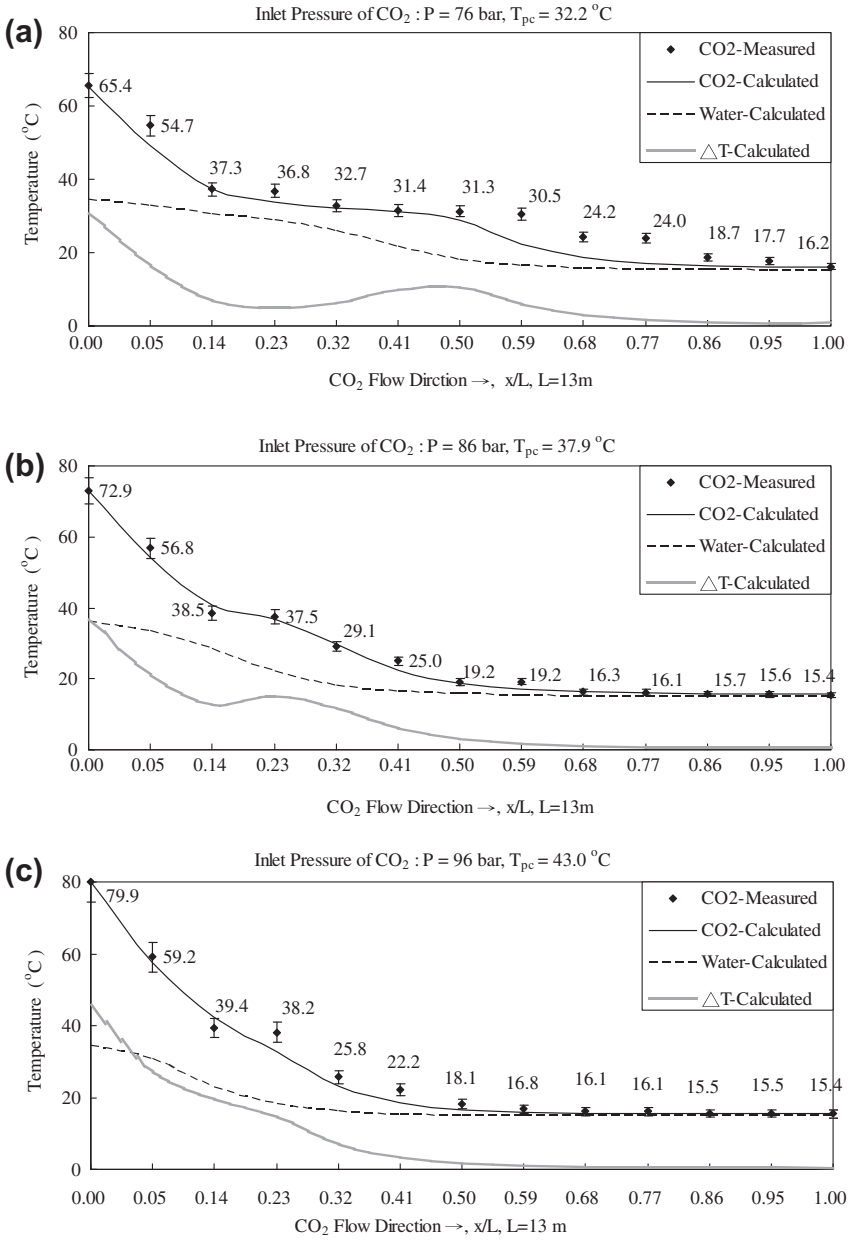

Fig. 6. Temperature distribution along the CO_2 refrigerant flow path at three various inlet pressure with a fixed cooling water inlet condition (2 L min^{-1}, 15 °C). (a) P = 76 bar; (b) P = 86 bar and (c) P = 96 bar.

experimental observation. The present simulations of the CO_2 temperature distribution, as shown in Fig. 6, are in line with the measurements. The foregoing results imply that the heat transfer characteristics of CO_2 nearby the pseudo critical region resemble normal refrigerants which show invariant temperature during condensation process. Hence, it would be beneficial to lengthen the influence of pseudo-critical region as far as heat transfer augmentation is concerned. Furthermore, the local heat transfer temperature difference between CO_2 and water decreases near the pseudo-critical points [21]. When the pressure is close to the critical value of 73.8 bar, the pinch point obviously occurs at the region where CO_2 pseudo-critical temperature takes place. The results are quite different from the traditional refrigerants to water heat exchangers with constant fluid property.

In addition, the drastic change C_P value for CO_2 also affects the distribution of the local heat transfer rate alongside the heat exchanger. Fig. 7(b) depicts a schematic showing the local heat transfer rate vs. dimensionless distance counting from the inlet of CO_2. It can be clearly seen in the figure, the heat transfer first decreases to a local minimum, followed by a rise to a plateau next to the minimum location, and finally decreased again toward the outlet. This strange phenomenon becomes more and more apparent when the inlet pressure is further reduced. In fact, a significant recovering of local heat transfer rate is encountered for P = 76 bar despite the maximum temperature difference still occurs at the CO_2 inlet.

Fig. 7(c) and (d) represents the variation of local heat transfer coefficient of CO_2 and water separately along the heat exchanger. When CO_2 passes through the pseudo-critical point, the local heat transfer coefficient of CO_2 rises rapidly then descends gradually toward the outlet whereas no detectable changes of heat transfer coefficients are found in the water side. As a consequence, the

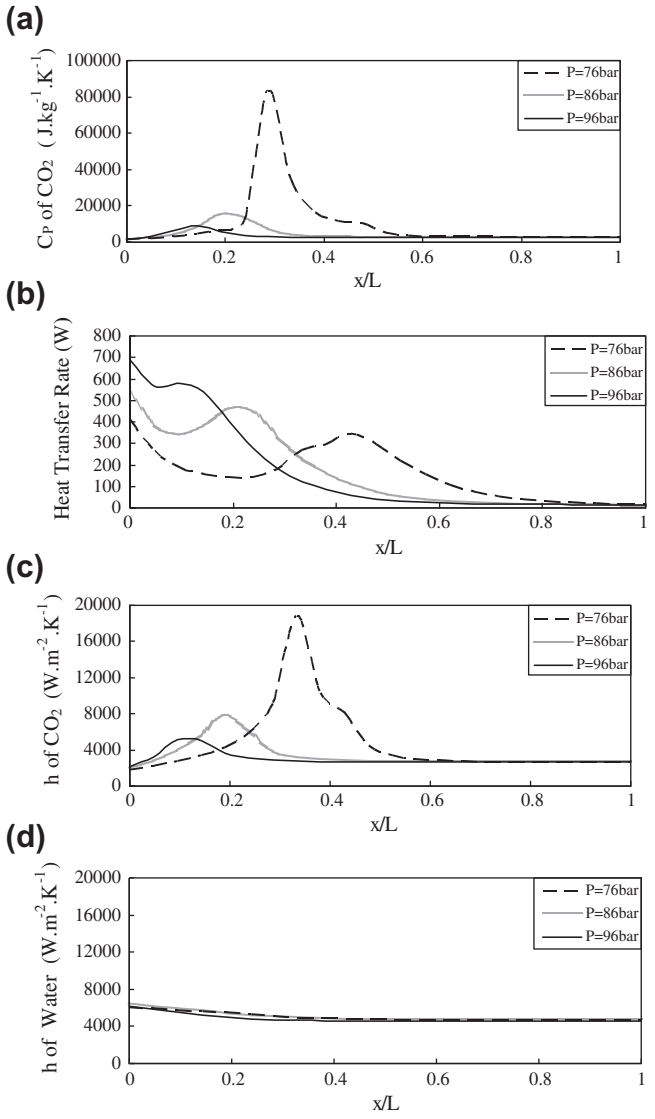

Fig. 7. Effect of CO_2 inlet pressure with a fixed cooling water inlet condition (2 L min^{-1}, 15 °C) on the (a) variation of *Cp* vs. dimensionless tube length; (b) variation of local heat transfer rate vs. dimensionless tube length; (c) variation of h_c vs. dimensionless tube length and (d) variation of h_w vs. dimensionless tube length.

dominant thermal resistance of the heat exchanger could switch to CO_2 side from water for a trans-critical process. Accordingly, near the pseudo-critical point, there is a significant local decrease in refrigerant-side thermal resistance which yields a sharp increase in local heating transfer duty [5,22]. This is quite distinct as compared to those of constant property fluids such as water to water heat exchangers. In summary, the drastic property changes of CO_2 occurs near the pseudo-critical region give rise to some special phenomena like small temperature drop and secondary peak of heat flux. Yet these phenomena may become even more pronounced when the pressure is close to the critical pressure.

5. Concluding remarks

In this study, an experiment is conducted to investigate the performance and heat transfer process of a supercritical CO_2 water-cooled gas cooler having tube-in-tube counter-flow configuration. The water is flowing in tube side whereas CO_2 is flowing at the annulus. The inlet pressures of the CO_2 are 76, 86, and 96 bar respectively. The temperature variation of the supercritical CO_2 alongside the heat exchanger and the corresponding heating capacity subject to water coolant flowrate are also reported. A tube-in-tube heat exchanger model applicable for supercritical fluid CO_2 is also developed to compare the test results. The measured total heating capacity ranges from 1.31 to 4.06 kW at various test conditions in this study. The calculations are in line with the experimental results with 94% of the 36 data points being within the ±20% accuracy limits. The results also show that the variation of CO_2 temperature drop tends to be very small when it is close to the pseudo-critical region when compared to that at the inlet region. Moreover this phenomenon becomes more pronounced as the inlet pressure is close to the critical pressure (73.8 bar). This is associated with the gigantic rise of heat capacity at the pseudo-critical region, and it corresponds to significant increase of heat transfer coefficient. The calculation also displays a peculiar phenomenon that the local heat transfer rate of the heat exchanger reveals a local maximum and minimum during the trans-critical process due to the drastic rise of specific heat (C_P value) of CO_2 nearby the pseudo-critical region.

Acknowledgements

The authors would like to express gratitude for the Energy R&D foundation funding from the Bureau of Energy of the Ministry of Economic, Taiwan. Part of the supporting from National Science Council under contract 102-ET-E-009-006-ET is also appreciated.

References

[1] M.H. Kim, J. Pettersen, C.W. Bullard, Fundamental process and system design issues in CO_2 vapor compression systems, Prog. Energy Combust. Sci. 30 (2004) 119–174.
[2] A. Pearson, Carbon dioxide new uses for an old refrigerant, Int. J. Refrig. 28 (2005) 1140–1148.
[3] J.M. Yin, C.W. Bullard, P.S. Hrnjak, R-744 gas cooler model development and validation, Int. J. Refrig. 24 (2001) 692–701.
[4] B.M. Fronk, S. Garimella, Water-coupled carbon dioxide microchannel gas cooler for heat pump water heaters: part I. Experiments, Int. J. Refrig. 34 (2011) 7–16.
[5] B.M. Fronk, S. Garimella, Water-coupled carbon dioxide microchannel gas cooler for heat pump water heaters: part II – model development and validation, Int. J. Refrig. 34 (2011) 17–28.
[6] E.A. Groll, J.H. Kim, Review of recent advances toward transcritical CO_2 cycle technology, HVAC&R Res. 13 (2007) 499–520.
[7] C. Dang, E. Hihara, In-tube cooling heat transfer of supercritical carbon dioxide part 1: experimental measurement, Int. J. Refrig. 24 (2004) 736–747.
[8] C. Dang, E. Hihara, In-tube cooling heat transfer of supercritical carbon dioxide. Part 2: Comparison of numerical calculation with different turbulence models, Int. J. Refrig. 24 (2004) 748–760.
[9] J. Sarkar, S. Bhattacharyya, M.R. Gopal, Simulation of a transcritical CO_2 heat pump cycle for simultaneous cooling and heating applications, Int. J. Refrig. 29 (2006) 735–743.
[10] J. Sarkar, S. Bhattacharyya, M. Ramgopal, A transcritical CO_2 heat pump for simultaneous water cooling and heating: test results and model validation, Int. J. Energy Res. 33 (2009) 100–109.
[11] L. Cecchinato, M. Corradi, S. Minetto, A critical approach to the determination of optimal heat rejection pressure in transcritical systems, Int. J. Refrig. 30 (2010) 1812–1823.
[12] P. Neksa, H. Rekstad, G.R. Zakeri, P.A. Schiefloe, CO_2-heat pump water heater: characteristics, system design and experimental results, Int. J. Refrig. 21 (1998) 172–179.
[13] P.C. Qi, Y.L. He, X.L. Wang, X.Z. Meng, Experimental investigation of the optimal heat rejection pressure for a transcritical CO_2 heat pump water heater, Appl. Therm. Eng. 56 (2013) 120–125.
[14] S.G. Wang, Y.N. He, H.F. Tuo, F. Gao, Z.W. Xing, Effect of heat transfer area and refrigerant mass flux in a gas cooler on heating performance of air-source transcritical CO_2 heat pump water heater system, Energy Build. 67 (2013) 1–10.
[15] D. Sanchez, R. Cabello, R. Llopis, E. Torrella, Development and validation of a finite element model for water–CO_2 coaxial gas-coolers, Appl. Energy 93 (2012) 637–647.
[16] REFPROP, 2007. Thermodynamic properties of refrigerants and refrigerant mixtures, version 8.0, Gaithersburg, M.D. National Institute of Standards and Technology, 2007.
[17] V. Gnielinsk, New equation for heat and mass transfer in turbulent pipe and channel flow, Int. J. Chem. Eng. 16 (1976) 359–368.

[18] S.M. Liao, T.S. Zhao, Measurements of heat transfer coefficients from supercritical carbon dioxide flowing in horizontal mini/micro channels, Int. J. Heat Transfer 124 (2002) 413–420.
[19] ISO/IEC Guide 98-3:2008, Uncertainty of measure – Part 3: Guide to the expression of uncertainty in measurement (GUM:1995).
[20] B.N. Taylor, C.E. Kuyatt, Guidelines for Evaluating and Expressing the Uncertainty of NIST Measurement Results, National Institute of Standards and Technology, 1994.
[21] J.F. Wang, E. Hihara, Study on carbon dioxide gas cooler heat transfer process under supercritical pressures, Int. J. Energy Res. 26 (2002) 1237–1251.
[22] P.Y. Yu, K.H. Lin, W.K. Lin, C.C. Wang, Performance of a tube-in-tube CO_2 gas cooler, Int. J. Refrig. 35 (2012) 2033–2038.